https://doi.org/10.2352/EI.2024.36.15.COIMG-132

Evaluation of Information Content in 2D and 3D Microstructural Characterization of Brush Particle-Based Hybrid Materials

Ayesha Abdullah[1], Kevin Ferguson[2], Lawrence Drummy[3], Levent Burak Kara[2], Michael R. Bockstaller[1]; [1]Carnegie Mellon University Department of Materials Science & Engineering, [2]Carnegie Mellon University Department of Mechanical Engineering, [3]Air Force Research Laboratory; [1,2]Pittsburgh, PA, [3]Fairborn, OH.

Abstract

In the field of polymers, 2D images are often used to discern information about the microstructure of bulk polymer materials. For brush particle assembly structures, this work evaluates microstructure information retrieved from different material characterization techniques for thin film (i.e., electron imaging of brush particle monolayers) and bulk materials (small angle X-ray scattering), respectively. The effect of confinement of polymer chains into thin (2D) films on the conformation of tethered chains is discussed and used to rationalize systematic discrepancies between characteristic nanoparticle spacings in thin films and bulk materials. An approach to rationalize bulk material properties based on thin film measurements is presented.

Introduction

The field of nanocomposites saw significant development around the turn of the century, motivated by the need for novel properties and functionalities for high-performance devices. Nanoparticle-assembled solids are formed from inorganic non-covalently bonded building blocks into colloidal or solid superlattices with unique, scale-dependent properties arising from confinement effects (molecular semiconductors), physical size and controllable microstructure (photonic crystals), and high surface-to-volume ratios (photovoltaics) [1]–[8]. Processing challenges in nanoparticle solids arising from weak cohesive forces between particles [9]–[11] drew attention to mechanically robust polymer-nanoparticle composites, where flexible, lightweight polymer serves as a matrix for the hybrid material, and allows easier processing techniques including extrusion, molding, and film-casting [12]–[14]. More recently, the advent of surface-initiated controlled radical polymerization (CRP) has enabled organic chains to be covalently bonded to the surface of inorganic nanoparticles; thus 'brush particles' represent a hybrid building block for controlled assembly of nanocomposite materials [15], [16]. Aided by a bonded polymer brush canopy that promotes dispersion interactions, brush particles assemble into materials with finer microstructural control and tunability than their unbonded counterparts, without inorganic aggregation [17]–[20].

Brush particles are a unique class of nanoscale particles, but studies have confirmed useful topological similarity to star polymers [21]–[24], where an impenetrable core is surrounded by radially extended polymer chains with varied effective segment density depending on the length and number of chains. In this context, polymer chain conformation models for brush particles emerged and were found to have strong influence on interparticle interactions and packing behavior. In seminal works by Likos on star polymers [25], [26], as well as Matsen & Kim [27] and Roan & Kawakatsu [28], [29] more specifically for brush particles, spherical brush topology was found to have interactions between hard and soft, dependent on the 'architecture' of the polymer canopy (a term used to describe manipulable parameters). Control of brush architecture thus enables mechanically robust materials with hard or soft sphere-like packing. High grafting densities causing stretched chains from strong excluded volume repulsion result in more rigid, FCC-like structures, while lower grafting densities where polymer chains adopt random-walk conformations tend to assemble amorphously. The latter characteristic elicited interest in brush particles as a candidate for the fabrication of 'hyperuniform' materials that were proposed by Torquato [30] to feature novel properties such as high efficiency photonic band formation of high mechanical strength. Simulations by Douglas & Chremos have suggested that the 'soft' polymer canopy suppresses long-range density fluctuations in brush particle material [31]. However, realization of hyperuniform states requires understanding of the effect of brush architecture and process conditions on the microstructure of the assembled material.

Nanocomposite materials test the limits of long-standing stereological procedures for microstructure evaluation, presenting a contemporary characterization challenge. While nanoparticle solids often assemble in crystalline and superlattice structures that can be observed and identified through procedures like electron microscopy and X-ray diffraction (XRD) [32], amorphous solids such as a-silicon and domain-forming polymeric materials require modified methods. Characteristic- or domain-sizing in amorphous but periodic polymer materials have been characterized in the past through micro-sectioning of bulk material and subsequent electron imaging. However, the fine control and precise conditions necessary to acquire a sufficient section (with electron-transparent thickness and large cohesive area) motivated a shift to easier thin-film casting methods such as spin-coating or drop-casting, and annealing [33]. These methods, while enabling suitable 2D materials for electron imaging, were not perfectly representative of bulk material due to surface interactions with both the air and substrate interfaces and defect formation during film formation [34]. On the other hand, 3D characterization methods were once restricted to bulk-averaged scattering (e.g., X-ray or neutron scattering). The onset of back-propagation algorithms driving automatic stereological calculations advanced the imaging field to developing tomography reconstructions of small 3D volumes of material imaged at series' of angles [35].

Along with each of these characterization techniques – electron imaging, scattering, and tomography – comes a unique set of microstructural information for inorganic/organic nanocomposites. Electron imaging can give a real-space view of particle spacings; however, the sampling area is small, and 2D films lack z-direction information, relying on stereological approximations from composition and structures within the observed window [36]. Scattering provides bulk-averaged microstructural characteristics, however the lack of analytical models for complex systems such as brush particles results in a heavy dependence on instrument resolution of data. Electron tomography appears to compromise

these two methods by providing direct observation of 3D microstructure, however true 3D volume reconstruction requires extremely difficult sectioning and is complicated by potential material degradation due to long electron beam exposure times [37]. To explore and contrast the information content of these methods and elucidate microstructural character of brush particle material, the following techniques were used to characterize a library of architecturally controlled PMMA-SiO_2 brush particle systems: TEM of monolayer material, and SAXS of bulk-thickness films.

Methods

Materials

Methyl methacrylate (MMA, Aldrich, 99%) was filtered through a basic alumina column to remove inhibitor. Silica nanoparticles dispersed in MIBK (MIBK-ST) with an average radius of 7.4±2.2nm were donated by Nissan Chemical. Copper(II) bromide ($CuBr_2$), Aldrich, 99%), anisole (Aldrich, 99%), dimethylformamide (DMF, Fisher, 99%), tin(II) 2-ethylhexanoate ($Sn(EH)_2$, 95%, Aldrich), tetrahydrofuran (THF, VWR 99%), and tris(1-(methylamino)ethyl)amine (ME_6TREN, Alfa, 99%) were used as received.

Synthesis of Brush Particles

Synthesis of 3-(chlorodimethylsilyl)propyl 2-bromoisobutyrate initiator and surface modification of silica nanoparticles was performed according to previously published work [15], [17]. The initiator-modified silica nanoparticles, MMA monomer, anisole, DMF, $CuBr_2$ and Me_6TREN were mixed in a sealed Schlenk flask while a solution of $Sn(EH)_2$ in anisole was prepared. Both solutions were nitrogen-purged. The $Sn(EH)_2$ solution was injected into the Schlenk flask to activate the catalyst complex and the flask was immediately placed in a 60°C oil bath. The monomer conversion and polymer molecular weight were monitored through TGA and SEC. Systematically high dispersity PMMA-SiO_2 particles were achieved by tuning [$CuBr_2$] according to [38]; concentrations less than 10ppm are able to achieve high dispersity, defined as $Đ$>1.5. The molecular parameters of the library of particles are tabulated in Table 1. Architectural parameters are defined as: ϕ_{PMMA} is the organic volume fraction of the material; N is the degree of polymerization of the polymer; M_N is the number average molecular weight; σ is the grafting density; $Đ$ is the dispersity index, where $Đ=M_W/M_N$.

Table 1. Molecular characteristics of PMMA-grafted silica (SiO_2) nanoparticles

Sample ID	Φ_{PMMA}	N	M_N (g/mol)	σ (chains/nm²)	Đ
N-*d*-1	0.86	159	15,930	0.66	1.26
N-*d*-2	0.96	763	76,270	0.63	1.32
N-*d*-3	0.92	351	35,120	0.62	1.29
N-*d*-4	0.94	482	48,180	0.59	1.28
N-*d*-5	0.96	822	82,230	0.55	1.29
N-*i*-1	0.86	313	31,300	0.35	1.25
N-*i*-2	0.91	526	52,570	0.35	1.24
N-*i*-3	0.91	722	72,160	0.25	1.34
N-*i*-4	0.88	642	64,200	0.20	1.30
N-*i*-5	0.91	957	95,690	0.18	1.30
N-*i*-6	0.77	353	36,690	0.16	1.25
H-*i*-1	0.87	484	48,400	0.25	2.04
H-*i*-2	0.90	551	55,070	0.30	1.59
H-*i*-3	0.71	228	22,790	0.19	1.68
H-*i*-4	0.82	317	31,680	0.26	1.76
H-*i*-5	0.81	327	32,650	0.23	1.63

Size Exclusion Chromatography (SEC)

Polymer chains were chemically cleaved from the surface of nanoparticles for SEC using the procedure detailed by previously published work [15]. Polymer number average M_N and weight average M_W molecular weights were determined using a Waters 515 pump and Waters 410 differential refractometer through PSS columns containing Styrogel at 10^5, 10^3, and 10^2 Å. THF was used as eluent at 35°C with a flow rate of 1mL/min. Linear PMMA was used as the calibration standard.

Thermogravimetric Analysis (TGA)

A TA Instruments 2950 was used to measure inorganic SiO_2 fraction with 4 steps: 1) jump to 120°C; 2) hold at 120°C for 10 minutes; 3) ramp up at 20°C/min to 800°C; 4) hold for 2 minutes. TGA plots were normalized to total weight after holding at 120°C and analyzed using TA Universal Analysis software.

Transmission Electron Microscopy (TEM)

Monolayer films were cast by dropping 8-10μL of 1-2mg/mL brush particle in toluene onto carbon coated copper grids. Particle microstructure was observed using a FEI Tecnai F20 electron microscope operated at 200kV. Images were taken on a Gatan Rio high resolution camera. Micrographs were filtered, and binarized using MATLAB's image processing toolbox.

Small Angle X-Ray Scattering (SAXS)

Bulk films were cast from highly concentrated (~40mg/mL) brush particle solutions in THF in a layer-by-layer process in PTFE molds, with average thickness of 0.2mm. Solvent evaporation between layers was slowed with a semi-closed system and vapor-supplied atmosphere. SAXS was performed on these films on a Xenocs Xeuss 3.0 with rotating anode copper source and Dectris Eiger2 detector (CMU Materials Characterization Facility) and Pilatus 3 300K detector (WPAFB). Background scattering from vacuum and linear PMMA were subtracted from resulting data to observe silica core interference patterns. 2D diffraction patterns were azimuthally averaged to 1D in XSACT software. Data analysis and transformation was performed in MATLAB.

Results & Discussion

TEM and the Radial Distribution Function

TEM micrographs of monolayers provide direct observation of particle positions to observe both uniformity and characteristic spacing of silica cores throughout the brush particle array. Previously published work used Voronoi analysis to describe uniformity of brush particle material, showing that while high grafting density with rigid polymer chains appeared more regular in structure, 'softer' intermediately grafted particles had a broader Voronoi cell size distribution indicating loss of order [17]. A more direct representation of characteristic distances and uniformity of

particulate material is the radial distribution function, *g(r)*. To determine this, large cohesive areas of film were imaged to obtain sufficient particle counts (>1000). An algorithm written in MATLAB using periodic boundary conditions produced interparticle distances that were placed in an area-normalized histogram. The resulting radial distribution function exhibits peaks at characteristic distances present in the system, where the magnitude reflects the frequency of that distance. Figure 1 exemplifies this analysis; the *g(r)* function shown was calculated from particle positions determined from the TEM micrograph, of which a subsection is shown. The brush particle films resulted in amorphous *g(r)* functions where a single characteristic peak appears, and second and third order distances are less significant, similar to *g(r)* calculated for amorphous liquids using Percus-Yevick approximation [39], [40]. The first peak of *g(r)* was used as an interparticle distance, d_{TEM}, corresponding to the radius at which the peak appears, to observe trends over architectural parameters compared to other characterization modes.

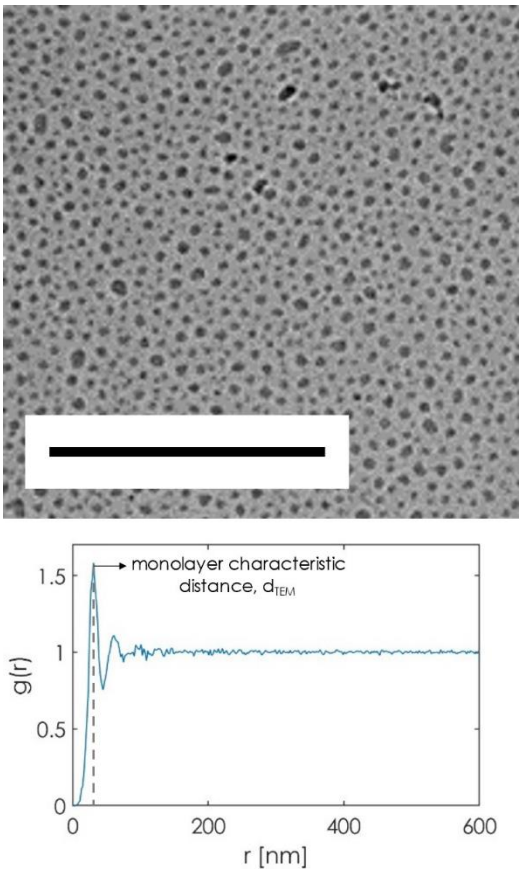

Figure 1. *Top: TEM micrograph of PMMA-SiO_2 sample N-i-1; scale bar is 500nm. A subsection of the micrograph is shown here to make nanoparticles (dark) easily visible to the eye. Bottom: Radial distribution function g(r) calculated from particle positions determined from the micrograph. Periodic boundary conditions were applied, with a maximum distance of half of the image size. The dotted line indicates the radius at which the characteristic peak appears.*

SAXS and the Structure Peak

SAXS experiments typically involve obtaining interference patterns of X-rays transmitted through a volume of scattering centers. Dilute solutions provide interference patterns containing information about the shape of the scattering center in question, while more 'concentrated' – or in this case bulk material – systems yield scattering center periodicity or order. The two can be related through Equation 1, where *I(q)* is the bulk interference pattern, *P(q)* is the form factor, *S(q)* is the structure factor, and $\Delta N/V$ is the difference in concentration per unit volume of scattering centers in the bulk and dilute materials.

$$I(q) = \Delta\frac{N}{V}S(q)P(q) \quad (1)$$

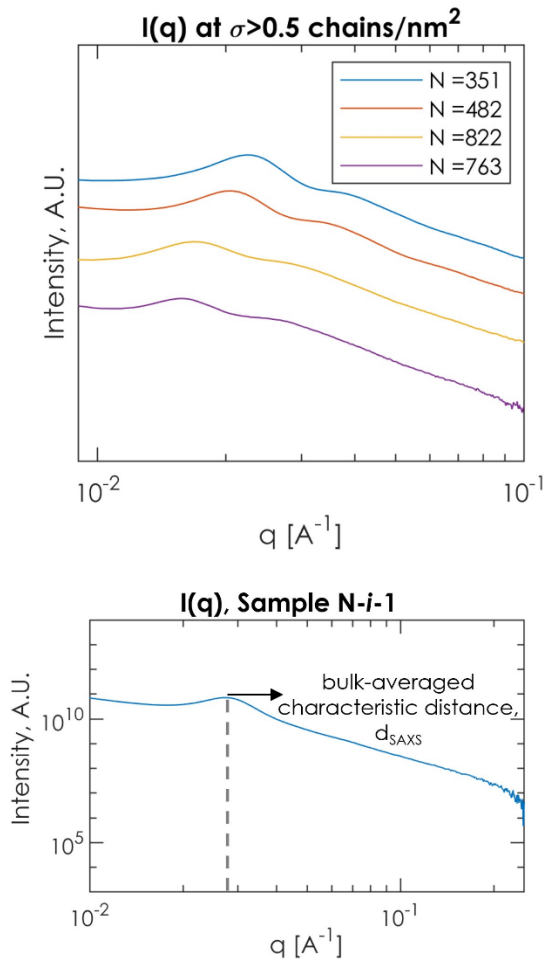

Figure 2. *(a) I(q) curves of solution-cast PMMA-SiO_2 bulk films with high grafting density (σ > 0.5nm^{-2}), narrow dispersity (Đ < 1.5), and varied degree of polymerization; background subtraction was used with vacuum and linear PMMA (35kg/mol) scattering, and curves shown here are scaled for visibility. (b) I(q) curve collected from PMMA-SiO_2 sample N-i-1 bulk film after background subtraction; the dotted line indicates the q-value at which a structure peak appears, which is converted to real-space distance using Equation 2.*

In the case of PMMA-SiO_2 brush particles, the silica core provides much stronger X-ray scattering than the PMMA surrounding it due to electron density. To eliminate background scattering from the PMMA canopy, scattering from linear PMMA of similar molecular weight (35kg/mol) was also collected and subtracted. Thus, *I(q)* interference patterns obtained in this way exhibited characteristics of silica positions within the material.

Systematic parameter variation allowed examination of *I(q)* scattering curves over the organic content of the brush particle material. Figure 2a compares *I(q)* (background-subtracted and re-scaled) of materials with consistent grafting density, narrow dispersity and varied molecular weight to observe the peak position as the polymer molecular weight (and consequentially, organic content) increased. The peak positions shifted to lower *q*-wavevectors, corresponding to increasing real-space distances, as *N* increased, indicating that as expected more organic material separated the silica cores, pushing them further apart and confirming that the first *I(q)* peak is a structure peak. This was also observed at lower grafting densities and increased dispersity. Thus, the *I(q)* peak position, converted to real-space using Equation 2, was used as a characteristic distance d_{SAXS} to observe architectural trends. This is exemplified in Figure 2b, for sample N-*i*-1.

$$d = \frac{2\pi}{q_{peak}} \tag{2}$$

Microstructural Trends

Both TEM micrographs of 2D monolayers and the bulk-averaged SAXS interference patterns yielded a characteristic distance observed in brush particle material. Previous studies by Ohno et al., Choi et al., and Lee et al. have confirmed that densely grafted brush particle materials exhibit polymer brush height scaling with degree of polymerization, *N*, dependent on grafting density [17], [22], [41]. Densely grafted systems tend to show brush height scaling of $N^{0.9}$ due to polymer chains being locally stretched from steric repulsions at high segment density. Intermediately grafted systems on the other hand exhibit brush height scaling of $N^{0.6}$, where segment density is lower, permitting random walk polymer conformation. Figures 3a and 3b illustrate the scaling observed at σ greater than 0.5 chains/nm^2 of PMMA-SiO_2 brush particles from both TEM of monolayers and SAXS of bulk material. Figures 3c and 3d contrast brush particles of intermediate σ, or less than 0.5 chains/nm^2. The scaling laws observed are consistent with theoretical calculations of two times PMMA brush height plus a 15nm SiO_2 core diameter (i.e., the entire brush particle diameter). As expected, the presence of locally stretched chains in high grafting density materials results in a larger logarithmic scaling coefficient than their intermediately grafted counterparts. This trend appears consistent regardless of 2D or 3D material, as does an expected increase in characteristic distance as the organic content (reflected in degree of polymerization *N* at controlled grafting density) increases.

Molecular weight dispersity introduces physical differences in the polymer canopy stemming from a positively skewed chain length distribution [42]. The presence of this 'tail' in the distribution results in most chains having length less than the number average, M_N, and thus a higher concentration of chain ends potentially contributing to larger fractional free volume. Figure 4 shows this phenomenon in the observed microstructures, where both TEM of monolayer (a) and SAXS of bulk material (b) exhibit larger characteristic distances in high dispersity PMMA-SiO_2 particles than their narrow dispersity counterparts, at the same organic content. The unique space-filling behavior of high dispersity brush canopies is captured in both 2D material and bulk-averaged 3D material.

Physical trends in the characteristic distance of brush particle microstructure over controlled grafting density, degree of polymerization, and dispersity are consistent in both planar and bulk material. However, systematic discrepancies between the characterization modes presented in Figures 3 and 4 are apparent. The magnitude of the characteristic distance measured from TEM of monolayers is larger than those measured from SAXS curves of particles with similar (or same) architecture.

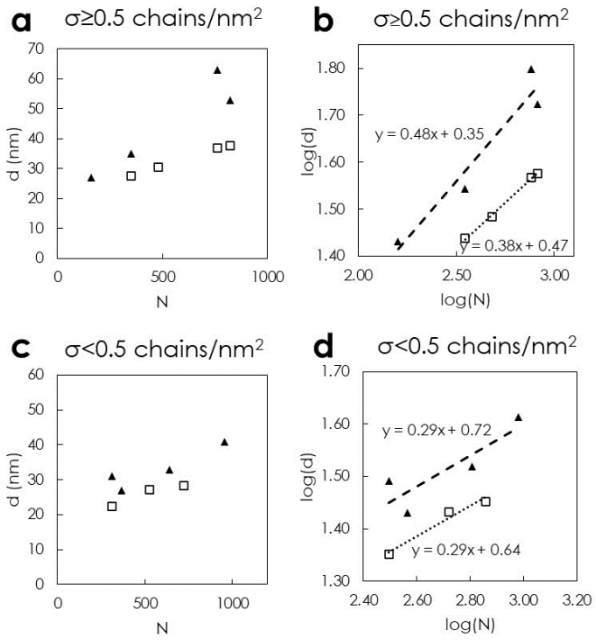

Figure 3. *(a) Characteristic distances for high grafting density (σ ≥ 0.5 chains/nm^2) PMMA-SiO_2 particles calculated from the position of the structure peak in I(q) measured from SAXS where $d_{SAXS} = 2\pi/q_{peak}$ (open squares) and from the position of the peak in g(r) determined from monolayer TEM micrographs $d_{TEM} = r_{g(r)\ peak}$ (filled triangles); (b) log-log plot of characteristic distances from (a) to determine N^x scaling where the slope of the linear fits shown correspond to x; the dotted line and dashed lines correspond to SAXS and TEM fits, respectively. (c) Characteristic distances for intermediate grafting density (σ < 0.5 chains/nm^2) PMMA-SiO_2 particles calculated in the same way as plot (a); (d) log-log plot of characteristic distances from (c) to determine N^x scaling using the same method as (b).*

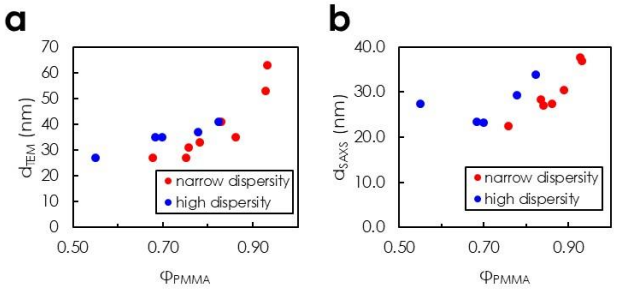

Figure 4. *(a) Characteristic distance calculated from g(r) from TEM of PMMA-SiO_2 monolayers; the distance corresponds to the peak position radius of g(r). (b) Characteristic distance calculated from the structure peak position of I(q) curves collected from PMMA-SiO_2 bulk films; the distance corresponds to $d_{SAXS} = 2\pi/q_{peak}$. High dispersity is classified as Đ ≥ 1.5 (blue), narrow dispersity is classified as Đ < 1.5 (red).*

TEM has long been used to observe polymer film morphology, and studies have shown that sample preparation plays a distinct role

in observations and measurements. For example, solvent affinity can influence domain morphologies, as evidenced by Li et al. in PS-*block*-PMMA diblock copolymers in mixtures of 1,1,2-trichloroethane and toluene [43]. Solvent interactions, casting mechanism, and surface interactions in both polymeric and nanocomposite materials can produce defects or entirely different morphologies. PMMA-SiO_2 brush particles are susceptible to these variations due to interactions with the polymer canopy. When cast as a 2D monolayer, the PMMA layer minimizes interfaces with air and the carbon substrate by taking a 'flattened' conformation favored by its relatively high surface tension compared to other commodity polymers [44]. This produces different particle distance as opposed to respective neat brush particle bulk material. Figure 5 shows the calculated ratio, d_{TEM}/d_{SAXS} between the characteristic distances observed in 2D monolayer and 3D bulk of identical PMMA-SiO_2 materials, and we find that the polymer expansion caused by surface interactions is approximately 30%, regardless of organic content or brush architecture.

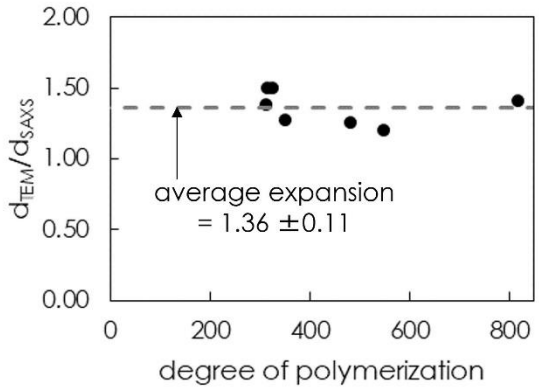

Figure 5. *Calculation of polymer expansion vs. degree of polymerization due to polymer morphology in a 2D monolayer film compared to 3D bulk material. The expansion is calculated as the ratio between d_{TEM} and d_{SAXS} which are defined in the text. The dotted line represents the average value of this ratio, calculated at 1.36 with a standard deviation of 0.11.*

Hyperuniformity

We have demonstrated that while 2D monolayer and 3D bulk film characterization methodologies both capture similar physical trends in the material, there are systematic differences in the magnitudes of characteristic length scales obtained by the two techniques. These differences can be interpreted as a consequence of the geometric constraints implied by thin film states. This raises the question of whether, in an isotropic amorphous material, there are microstructurally relevant properties that can be determined from both methods, independent of stereological differences. One such property is hyperuniformity. Torquato presented a versatile definition deriving from the structure factor of materials (determined through either imaging or scattering experiments) near the zero wavelength limit [45].

The relationship compares the characteristic distance defined by the first structure peak *S(peak)* with long-range material density captured in the zero-limit at *S(q=0)*. Thus, the hyperuniformity parameter ***h*** decreases with long-wavelength density fluctuations. Equation 3 defines the practical limit that characterizes hyperuniform materials.

$$\boldsymbol{h} = \frac{S(q=0)}{S(peak)} < 10^{-3} \tag{3}$$

This hyperuniform character of brush particle assemblies was examined over a range of architectural parameters including N, σ, and $Đ$ in 2D monolayers of PMMA-SiO_2 brush particles using the radial distribution function *g(r)*. First, a two-dimensional Fourier Transform was performed on the *g(r)* functions using Equation 4 to obtain the structure factor *S(q)*,

$$S(q) = 1 + 2\pi\rho \int_0^\infty (g(r) - 1) J_0(qr) r dr \tag{4}$$

where ρ is the number density of particles by volume, and $J_0(qr)$ is the zero-order Bessel function of the first kind. Subsequently ***h*** was determined from Equation 3.

Preliminary results from calculation of ***h*** using this method are presented in Figure 6. Previous studies by Chremos & Douglas proposed that brush particles with 'softer' polymer canopies, i.e., with intermediate grafting densities (to avoid locally stretched chains) and chain lengths enabling entanglement formation favored hyperuniform character [31]. Interestingly, results from monolayers generally agree for high dispersity PMMA-SiO_2 systems where larger molecular weights result in lower ***h***, however narrow dispersity systems appear to have a limiting molecular weight to this behavior, regardless of grafting density.

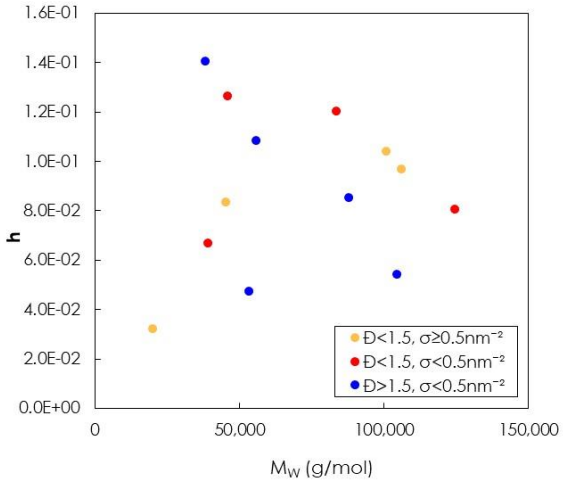

Figure 6. *Hyperuniformity, **h**, of PMMA-SiO_2 brush particles over weight average molecular weight M_W. Yellow points are materials with narrow dispersity (Đ<1.5) and high grafting density (σ≥0.5 chains/nm²); red points are materials with narrow dispersity (Đ<1.5) and intermediate grafting density (σ<0.5 chains/nm²); blue points are materials with high dispersity (Đ>1.5) and intermediate grafting density (σ<0.5 chains/nm²).*

Conclusions

The primary focus of this work was to analyze and compare microstructure data obtained through thin film and bulk material characterization techniques, specifically in the context of brush particle systems. Thin films were characterized by electron imaging, while bulk materials small angle X-ray scattering. For each method, microstructure-related properties such as radial distribution, structure factor, characteristic distance, and hyperuniformity were considered. Characteristic distance was shown to increase with increasing degree of polymerization, regardless of dispersity or

grafting density. Importantly, the discrepancy in this quantity between monolayer and bulk material agreed with the expected 2D-3D discrepancy. Our results demonstrate that the packing constraints in thin films can alter characteristic spacings and thus the information retrieved from the analysis of thin and thick film geometries. The impact of these packing constraints is that structure characteristics obtained from bulk (X-ray scattering or electron tomography) and thin film measurements (TEM) cannot be brought to congruence by application of, for example, stereological analysis. For the example of brush particles, we demonstrate reconciliation of 2D and 3D results by considering the role of interface energy on the film topography and particle distance. Hence, structure characterization using multimodal analysis was accomplished.

Some aspects of this work merit additional investigation. For example, *I(q)* provides a convenient means to determine the characteristic distance, however a better representation could be obtained by collecting a coherent brush particle form factor and using the relation outlined in Equation 1 to compute a corresponding structure factor. This would allow for the correction of errors due to shape scattering, raise the resolution of the technique, and enable its application to determine more refined structural parameters such as the degree of hyperuniformity.

References

[1] Z. Wu, J. Chen, and R. Jin, "One-Pot Synthesis of Au25(SG)18 2- and 4-nm Gold Nanoparticles and Comparison of their Size-Dependent Properties," *Adv. Funct. Mater.*, vol. 21, pp. 177–183, 2011, doi: 10.1002/adfm.201001120.

[2] C. Salzemann, I. Lisiecki, A. Brioude, and J. Urban, "Collections of Copper Nanocrystals Characterized by Different Sizes and Shapes: Optical Response of These Nanoobjects," *J. Phys. Chem. B*, vol. 108, pp. 13242–13248, 2004, doi: 10.1021/jp048491n.

[3] S. Kim, S. Y. Lee, S. Yang, and G. Yi, "Self-assembled colloidal structures for photonics," *NPG Asia Mater.*, vol. 3, no. January, pp. 25–33, 2011, doi: 10.1038/asiamat.2010.192.

[4] E. V. Shevchenko, D. V. Talapin, N. A. Kotov, S. O'Brien, and C. B. Murray, "Structural diversity in binary nanoparticle superlattices," *Nature*, vol. 439, no. 7072, pp. 55–59, 2006, doi: 10.1038/nature04414.

[5] N. Vogel, M. Retsch, C.-A. Fustin, A. del Campo, and U. Jonas, "Advances in Colloidal Assembly: The Design of Structure and Hierarchy in Two and Three Dimensions," *ACS Chem. Rev.*, vol. 115, p. 6265−6311, 2015, doi: 10.1021/cr400081d.

[6] Y. Min, M. Akbulut, K. Kristiansen, Y. Golan, and J. Israelachvili, "The role of interparticle and external forces in nanoparticle assembly," *Nat. Mater.*, vol. 7, no. July, pp. 527–538, 2008.

[7] M. A. Boles, M. Engel, and D. V Talapin, "Self-Assembly of Colloidal Nanocrystals: From Intricate Structures to Functional Materials," *ACS Chem. Rev.*, vol. 116, p. 11220−11289, 2016, doi: 10.1021/acs.chemrev.6b00196.

[8] C. B. Murray, C. R. Kagan, and M. G. Bawendi, "Synthesis and Characterization of Monodisperse Nanocrystals and Close-Packed Nanocrystal Assemblies," *Annu. Rev. Mater. Res.*, vol. 30, pp. 545–610, 2000, doi: 10.1146/annurev.matsci.30.1.545.

[9] J. H. Prosser, T. Brugarolas, S. Lee, A. J. Nolte, and D. Lee, "Avoiding cracks in nanoparticle films," *Nano Lett.*, vol. 12, no. 10, pp. 5287–5291, 2012, doi: 10.1021/nl302555k.

[10] B. Hatton, L. Mishchenko, S. Davis, K. H. Sandhage, and J. Aizenberg, "Assembly of large-area, highly ordered, crack-free inverse opal films," *Proc. Natl. Acad. Sci.*, vol. 107, no. 23, pp. 10354–10359, 2010, doi: 10.1073/pnas.1000954107.

[11] V. R. Dugyala, H. Lama, D. K. Satapathy, and M. G. Basavaraj, "Role of particle shape anisotropy on crack formation in drying of colloidal suspension," *Sci. Rep.*, vol. 6, pp. 1–7, 2016, doi: 10.1038/srep30708.

[12] S. Li, M. Meng Lin, M. S. Toprak, D. K. Kim, and M. Muhammed, "Nanocomposites of polymer and inorganic nanoparticles for optical and magnetic applications," *Nano Rev.*, vol. 1, no. 1, p. 5214, 2010, doi: 10.3402/nano.v1i0.5214.

[13] C. Sanchez, B. Julián, P. Belleville, and M. Popall, "Applications of hybrid organic-inorganic nanocomposites," *J. Mater. Chem.*, vol. 15, no. 35–36, pp. 3559–3592, 2005, doi: 10.1039/b509097k.

[14] V. Viswanathan, T. Laha, K. Balani, A. Agarwal, and S. Seal, "Challenges and advances in nanocomposite processing techniques," *Mater. Sci. Eng. R Reports*, vol. 54, no. 5–6, pp. 121–285, 2006, doi: 10.1016/j.mser.2006.11.002.

[15] J. Pyun, S. Jia, T. Kowalewski, G. D. Patterson, and K. Matyjaszewski, "Synthesis and characterization of organic/inorganic hybrid nanoparticles: Kinetics of surface-initiated atom transfer radical polymerization and morphology of hybrid nanoparticle ultrathin films," *Macromolecules*, vol. 36, no. 14, pp. 5094–5104, 2003, doi: 10.1021/ma034188t.

[16] J. Yan, M. R. Bockstaller, and K. Matyjaszewski, "Brush-modified materials: Control of molecular architecture, assembly behavior, properties and applications," *Prog. Polym. Sci.*, vol. 100, p. 101180, 2020, doi: 10.1016/j.progpolymsci.2019.101180.

[17] J. Lee *et al.*, "Molecular Parameters Governing the Elastic Properties of Brush Particle Films," *Macromolecules*, vol. 53, no. 4, pp. 1502–1513, 2020, doi: 10.1021/acs.macromol.9b01809.

[18] M. J. A. Hore, "Polymers on nanoparticles: structure & dynamics," *Soft Matter*, vol. 15, no. 6, pp. 1120–1134, 2019, doi: 10.1039/C8SM02110D.

[19] O. Azzaroni, "Polymer brushes here, there, and everywhere: Recent advances in their practical applications and emerging opportunities in multiple research fields," *J. Polym. Sci. Part A Polym. Chem.*, vol. 50, no. 16, pp. 3225–3258, 2012, doi: 10.1002/pola.26119.

[20] K. Ohno, K. Koh, Y. Tsujii, and T. Fukuda, "Fabrication of ordered arrays of gold nanoparticles coated with high-density polymer brushes," *Angew. Chemie - Int. Ed.*, vol. 42, no. 24, pp. 2751–2754, 2003, doi: 10.1002/anie.200250850.

[21] K. Ohno, T. Morinaga, S. Takeno, Y. Tsujii, and T. Fukuda, "Suspensions of silica particles grafted with concentrated polymer brush: A new family of colloidal crystals," *Macromolecules*, vol. 39, no. 3, pp. 1245–1249, Feb. 2006, doi: 10.1021/ma0521708.

[22] J. Choi, C. M. Hui, J. Pietrasik, H. Dong, K. Matyjaszewski, and M. R. Bockstaller, "Toughening fragile matter: Mechanical properties of

particle solids assembled from polymer-grafted hybrid particles synthesized by ATRP," *Soft Matter*, vol. 8, no. 15, pp. 4072–4082, 2012, doi: 10.1039/c2sm06915f.

[23] D. Vlassopoulos and G. Fytas, "From polymers to colloids: Engineering the dynamic properties of hairy particles," *Adv. Polym. Sci.*, vol. 236, no. December 2009, pp. 1–54, 2010, doi: 10.1007/12-2009-31.

[24] M. Giovino, J. Pribyl, B. Benicewicz, S. Kumar, and L. Schadler, "Linear rheology of polymer nanocomposites with polymer-grafted nanoparticles," *Polymer (Guildf).*, vol. 131, pp. 104–110, 2017, doi: 10.1016/j.polymer.2017.10.016.

[25] C. N. Likos *et al.*, "Ordering phenomena of star polymer solutions approaching the Θ state," *Phys. Rev. E - Stat. Physics, Plasmas, Fluids, Relat. Interdiscip. Top.*, vol. 58, no. 5, pp. 6299–6307, 1998, doi: 10.1103/PhysRevE.58.6299.

[26] C. N. Likos *et al.*, "Star Polymers Viewed as Ultrasoft Colloidal Particles," *Phys. Rev. Lett.*, vol. 80, no. 20, pp. 4450–4453, 1998, doi: 10.1103/PhysRevLett.80.4450.

[27] J. U. Kim and M. W. Matsen, "Interaction between polymer-grafted particles," *Macromolecules*, vol. 41, no. 12, pp. 4435–4443, 2008, doi: 10.1021/ma8002856.

[28] J. R. Roan and T. Kawakatsu, "Self-consistent-field theory for interacting polymeric assemblies. I. Formulation, implementation, and benchmark tests," *J. Chem. Phys.*, vol. 116, no. 16, pp. 7283–7294, 2002, doi: 10.1063/1.1463424.

[29] J. R. Roan and T. Kawakatsu, "Self-consistent-field theory for interacting polymeric assemblies. II. Steric stabilization of colloidal particles," *J. Chem. Phys.*, vol. 116, no. 16, pp. 7295–7310, 2002, doi: 10.1063/1.1463425.

[30] S. Torquato and F. H. Stillinger, "Local density fluctuations, hyperuniformity, and order metrics," *Phys. Rev. E - Stat. Physics, Plasmas, Fluids, Relat. Interdiscip. Top.*, vol. 68, no. 4, pp. 1–25, 2003, doi: 10.1103/PhysRevE.68.041113.

[31] A. Chremos and J. F. Douglas, "Particle localization and hyperuniformity of polymer-grafted nanoparticle materials," *Ann. Phys.*, vol. 529, no. 5, pp. 1–13, 2017, doi: 10.1002/andp.201600342.

[32] S. Mourdikoudis, R. M. Pallares, and N. T. K. Thanh, "Characterization techniques for nanoparticles: Comparison and complementarity upon studying nanoparticle properties," *Nanoscale*, vol. 10, no. 27, pp. 12871–12934, 2018, doi: 10.1039/c8nr02278j.

[33] G. H. Michler, *Electron Microscopy of Polymers*. Berlin, Heidelberg: Springer Berlin Heidelberg, 2008. doi: 10.1007/978-3-540-36352-1.

[34] R. Adhikari, "Electron Microscopic Analysis of Multicomponent Polymers and Blends," *Charact. Polym. Blends Miscibility, Morphol. Interfaces*, vol. 9783527331, pp. 551–578, 2015, doi: 10.1002/9783527645602.ch17.

[35] D. N. Mastronarde, "Dual-axis tomography: An approach with alignment methods that preserve resolution," *J. Struct. Biol.*, vol. 120, no. 3, pp. 343–352, 1997, doi: 10.1006/jsbi.1997.3919.

[36] E. E. Underwood, *Quantitative Stereology*. Reading, Massachusetts: Addison-Wesley Publishing Company, 1970.

[37] P. Singh, B. R. Venugopal, and D. R. Nandini, "Effect of Electron Beam Irradiation on Polymers," *J. Mod. Mater.*, vol. 5, no. 1, pp. 24–33, 2018, doi: 10.21467/jmm.5.1.24-33.

[38] Z. Wang *et al.*, "Control of Dispersity and Grafting Density of Particle Brushes by Variation of ATRP Catalyst Concentration," *ACS Macro Lett.*, vol. 8, no. 7, pp. 859–864, 2019, doi: 10.1021/acsmacrolett.9b00405.

[39] J.-P. Hansen and I. R. McDonald, *Theory of Simple Liquids*, 3rd ed. Elsevier, 2006. doi: 10.1016/B978-0-12-370535-8.X5000-9.

[40] D. J. Kinning and E. L. Thomas, "Hard-Sphere Interactions between Spherical Domains in Diblock Copolymers," *Macromolecules*, vol. 17, pp. 1712–1718, 1984, doi: 10.1021/ma00139a013.

[41] K. Ohno, T. Morinaga, S. Takeno, Y. Tsujii, and T. Fukuda, "Suspensions of silica particles grafted with concentrated polymer brush: Effects of graft chain length on brush layer thickness and colloidal crystallization," *Macromolecules*, vol. 40, no. 25, pp. 9143–9150, 2007, doi: 10.1021/ma071770z.

[42] P. Cassagnau, J. P. Montfort, G. Marin, and P. Monge, "Rheology of polydisperse polymers: relationship between intermolecular interactions and molecular weight distribution," *Rheol. Acta*, vol. 32, no. 2, pp. 156–167, 1993, doi: 10.1007/BF00366679.

[43] Y. Li, H. Huang, T. He, and Y. Gong, "The effect of the preferential affinity of the solvent on the microstructure of solution-cast block copolymer thin films," *J. Phys. Chem. B*, vol. 114, no. 3, pp. 1264–1270, 2010, doi: 10.1021/jp908852u.

[44] T. Hata and T. Kasemura, "Surface and Interfacial Tensions of Polymer Melts and Solutions.," *Polym. Sci. Technol.*, vol. 12 A, no. 9, pp. 15–41, 1980, doi: 10.1007/978-1-4613-3093-6_3.

[45] S. Torquato, "Disordered hyperuniform heterogeneous materials," *J. Phys. Condens. Matter*, vol. 28, no. 41, 2016, doi: 10.1088/0953-8984/28/41/414012.